Microsyst Technol (2018) 24:1041–1051
https://doi.org/10.1007/s00542-017-3459-9

TECHNICAL PAPER

Energy management strategy to simplify the hardware structure of wireless sensor nodes

Yiyuan Zhang[1,2,3,4] · Jiahao Zhao[1,2,3,4] · Yajiang Yin[1,2,3,4] · Zheng You[1,2,3,4,5]

Received: 26 May 2017 / Accepted: 26 May 2017 / Published online: 15 June 2017

Abstract Maximum power point tracking (MPPT) circuits in photovoltaic (PV) cell-based wireless sensor nodes often make the systems complex and costly. This paper proposes a novel energy management strategy for PV cell-based systems to remove their MPPT circuit without reducing their working efficiency. By modeling the non-MPPT system, energy storage in different situations is calculated. The key factors to improve the working efficiency of the system, such as operating voltage and number of PV cells in series, are also analyzed. A design is proposed to maximize the working efficiency. Another model for systems including MPPT circuits is also proposed for comparison. Simulation analysis shows that during the monitoring period, the total active time of the non-MPPT system can be as long as that of the system with MPPT circuits. Experimental tests confirm the validity of the proposed energy strategy. More importantly, the number of electronic components in the non-MPPT system's power module is only approximately 1/5 of that of the other system. This strategy provides a possible approach for practical wireless sensor nodes that are small in size and have low cost.

Electronic supplementary material The online version of this article (doi:10.1007/s00542-017-3459-9) contains supplementary material, which is available to authorized users.

✉ Jiahao Zhao
falxon@mail.tsinghua.edu.cn

✉ Zheng You
yz-dpi@mail.tsinghua.edu.cn

Yiyuan Zhang
yy-zhang13@mails.tsinghua.edu.cn

Yajiang Yin
yin-yj14@mails.tsinghua.edu.cn

[1] State Key Laboratory of Precision Measurement Technology and Instruments, Tsinghua University, Beijing 100084, People's Republic of China

[2] Department of Precision Instrument, Tsinghua University, Beijing 100084, People's Republic of China

[3] Beijing Innovation Center for Future Chip, Tsinghua University, Beijing 100084, People's Republic of China

[4] Collaborative Innovation Center for Micro/Nano Fabrication, Device and System, Tsinghua University, Beijing 100084, People's Republic of China

[5] Tsinghua-Berkeley Shenzhen Institute, University Town of Shenzhen, Shenzhen 518055, People's Republic of China

1 Introduction

With the rapid development of the internet of things, there is an increasing demand for wireless sensor networks (WSNs) (Gubbi et al. 2013). Since a WSN is composed of a large number of wireless sensor nodes to monitor a large area, the cost and installation of nodes should be as low as possible to make the WSN reasonable (Potdar et al. 2009). Therefore, WSNs with small-sized and low-cost nodes are becoming the mainstream (Botta et al. 2016; Jang et al. 2016). In most cases, the power module of the node occupies a considerable part of the whole system (Chou et al. 2016; Guan et al. 2017). Moreover, due to the limited size of nodes, power module is unable to provide too much energy, which causes a serious problem of power limitation, and researchers have to make WSNs more complex in either hardware or software (Gandelli et al. 2005; Razzaque and Dobson 2014). Thus, the optimization of the power modules is a practical approach to reduce both the size and cost of nodes.

Since photovoltaic (PV) cells have high power density, they have become one of the most commonly used energy

harvesters in wireless sensor nodes. Among all the PV cell-based nodes, nearly every system uses the maximum power point tracking (MPPT) techniques to maximize the amount of power harvested and assist the load to collect more environmental data (Raghunathan et al. 2005; Simjee and Chou 2006; Brunelli et al. 2008, 2009; Hassanalieragh et al. 2014; Li et al. 2014;). One of the most well-known techniques is called the fractional open-circuit voltage (FOC) method, which limits the output voltage of PV module to about 75% of its open-circuit voltage. Unfortunately, the MPPT techniques usually require an additional circuit, making the system more complex, and the circuit also consumes energy to carry out its function (Han et al. 2008; Lu et al. 2010). The MPPT circuit in the wireless sensor nodes is contrary to the principle of being small and low-cost. However, the working efficiency of systems without the MPPT circuit is relatively low, and these systems have to sleep longer to collect energy, which is disadvantageous for monitoring (Minami et al. 2005). In conclusion, a method to remove the complex MPPT circuit without reducing working efficiency is lacking.

We propose a novel energy management strategy to solve the current problem. It optimizes the working efficiency of systems without an MPPT circuit so that the small-sized and low-cost system can replace it with a complex circuit. An energy model is established for systems without an MPPT circuit that shows the energy storage in different conditions. Based on the working mode durations analyzed by the model, an optimized strategy is proposed to maximize the load's active time in one working period. Simulation of the load's working process is conducted, and the total active time is calculated to be as long as that of the traditional system that includes the MPPT circuit. Experimental tests are conducted using a Solar Simulator, which verifies the strategy. Systems without an MPPT circuit have fewer electronic components, making them smaller and more affordable. The energy strategy optimizes their working efficiency to be comparable to that of traditional systems. Therefore, our work provides an effective solution to exclude the MPPT circuit for ultra-small-sized and low-cost wireless sensor nodes such as smart dusts (Kahn et al. 1999).

2 System modeling

Due to their long life cycle, relative high energy density and power density (Namisnyk and Zhu 2003), supercapacitors are becoming widely used working with PV cells to power wireless sensor nodes (Minami et al. 2005; Simjee and Chou 2006; Hassanalieragh et al. 2014). The hardware structure of nodes without an MPPT circuit is shown in Fig. 1a, while Fig. 1b depicts the most common structure. The simple system, a non-MPPT system, is composed of the following devices: PV cells for energy harvesting from the environment, a diode for damage protection of PV cells from current backflow, a supercapacitor for energy storage and output, a DCDC for provision of stable voltage, and a load for environmental monitoring. The traditional system, an MPPT system, includes an additional MPPT circuit that usually consists of DCDCs, comparators and diodes.

In wireless sensor nodes, loads usually fluctuate between sleeping mode and active mode in the most typical way (Penella and Gasulla 2007). Here, $T_{active}/(T_{sleep} + T_{active})$ in one working period is defined as R_a, which describes the duty ratio of the active mode. The system's total active time is longer over a long period of time with a higher R_a, which means it can collect more environmental information. Therefore, the energy management strategy is designed to search the system parameters to maximize R_a, and improve the maximum working efficiency of the non-MPPT system. A model for the non-MPPT system is established to analyze the energy storage and to calculate R_a under different working conditions. A similar model for the MPPT system is also established to compare the R_a values of the two different systems that help in evaluating the strategy.

2.1 Model of the non-MPPT system

The governing equations of the general system model (Eqs. 1–3) are derived from Kirchhoff's laws and the properties of DCDC.

$$V_{pv} - V_{Diode} = V_{SC} \tag{1}$$

$$I_{pv} = I_{Diode} \tag{2}$$

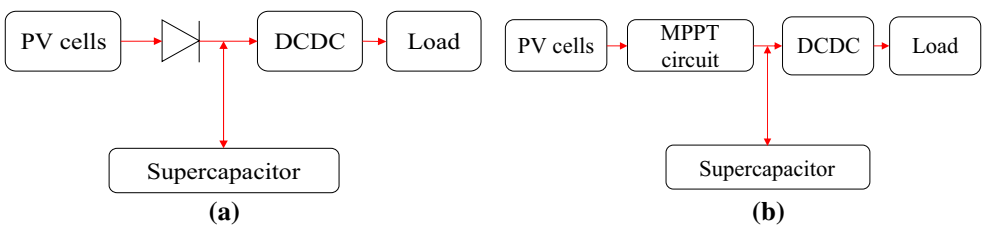

Fig. 1 Hardware structure of wireless sensor nodes based on PV cells and supercapacitors: **a** the non-MPPT system; **b** the MPPT system

$$V_{SC} \times (I_{Diode} + I_{SC}) \times \eta_{DCDC} = V_{load} \times I_{load} \quad (3)$$

V_{pv} and I_{pv} are the output voltage and output current of the PV cells. V_{SC} is the output voltage of the supercapacitor, and I_{SC} is the output current of the supercapacitor when it is positive and represents the charging current of the supercapacitor when it is negative. The instantaneous forward voltage of the diode is V_{Diode}, and I_{Diode} is its forward current. These parameters are variable and changeable under different circumstances. η_{DCDC} and V_{load} are the transfer efficiency and output voltage of DCDC, and I_{load} is the load current. The former three parameters are determined by specific devices.

2.1.1 Model of PV cells

The single diode equivalent circuit, as shown in Fig. 2, is used to develop the current–voltage (I-V) characteristic equation (Eq. 4) of PV cells (Dzimano 2008).

$$I_{pv} = I_L - I_{sat}\left[exp\left(\frac{V_{pv} + I_{pv} \times R_s}{\alpha}\right) - 1\right] - \frac{V_{pv} + I_{pv} \times R_s}{R_{sh}} \quad (4)$$

There are five parameters in the model: I_L is the light current, I_{sat} is the reverse saturation current of the diode, α is the ideality factor, R_s is the series resistance, and R_{sh} is the shunt resistance.

These five parameters can be calculated according to environmental conditions, including solar radiance G, air temperature T and air mass AM, and their values under standard rating conditions are SRC with G* = 1000 W/m^2, T* = 25 °C and AM* = 1.5 (Dzimano 2008).

2.1.2 Model of the diode

The current–voltage characteristic of diodes can be described by the Shockley function.

$$I_{Diode} = A \times (\exp(B \times V_{Diode}) - 1) \quad (5)$$

The two parameters, A and B, can be calculated based on the datasheet.

2.1.3 Model of the supercapacitor

Common double-layer supercapacitor characteristics can be described by the two-branch RC network (Zubieta and Bonert 2000) shown in Fig. 3.

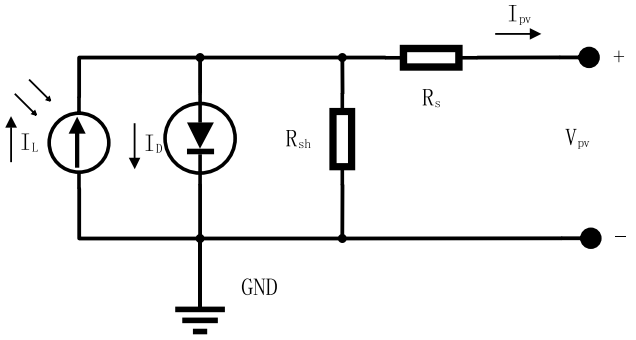

Fig. 2 Single diode circuit for the model of PV cells

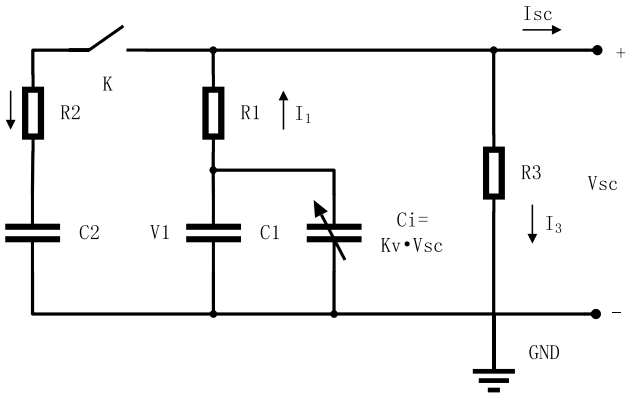

Fig. 3 Two-branch RC network for supercapacitor model

Resistance R_3 reflects the leakage of the supercapacitor. The first branch, consisting of R_1, C_1 and C_i, interprets the transient stage of charging or discharging. The second branch, consisting of R_2 and C_2, interprets the charge redistribution process during the retardant stage. Here, a switch K is involved that is open to disconnect the second branch when the supercapacitor works without a retardant stage. In the non-MPPT system, the supercapacitor is always in the quick charging or discharging state, meaning that K is always open. Equations 6–9 describe the transient stage of the supercapacitor. All the parameters can be determined from a constant current test.

$$I_{SC}(t) = I_1(t) - I_3(t) \quad (6)$$

$$V_{SC}(t) = I_3(t) \times R_3 \quad (7)$$

$$V_{SC}(t) = V_1(t) - I_1(t) \times R_1 \quad (8)$$

$$-I_1(t) = \frac{dV_1(t)}{dt}(C_1 + K_V \times V_{SC}(t)) \quad (9)$$

2.1.4 Model of DCDC and load

η_{DCDC} and V_{load} are usually given by the datasheet of DCDC; the different load current I_{load} in different working modes can be tested.

2.2 Model of MPPT system

The general system model of the MPPT systems is based on the energy conservation law instead of Kirchhoff's laws. The governing equation for the MPPT system is as follows:

$$(P_{pv} \times \cdot \eta_{MPPT} + P_{SC}) \times \eta_{DCDC} = P_{load} \quad (10)$$

P_{pv} and P_{SC} are the output voltage of the PV cells and supercapacitor, η_{MPPT} is the conversion efficiency of the MPPT circuit, and P_{load} is the power consumption of the load.

The PV cells and supercapacitor models of the MPPT system are based on the non-MPPT system models, and models of DCDC and load are the same as those of the non-MPPT system.

2.2.1 Model of PV cells

When the environmental parameters are input into the model of PV cells in chapter 2.1.1, the functional relationship between PV cell output power and output voltage can be determined; P_{pv} in Eq. 14 is the maximum power value of the function. The diode that protects PV cells from current backflow damage is integrated into the MPPT circuit during the modeling of PV cells, and η_{MPPT} is tested by a charging test (Enslin 1990).

2.2.2 Model of the supercapacitor

V_1, the voltage across the first branch's capacitors, can be approximately regarded as V_{SC} because the product of current and resistance in the first branch is usually much smaller than V_1 (shown in Eq. 8). In the models of the MPPT system, V_1 is used to replace V_{SC} to simplify the computation.

3 Optimization and simulation

The models are developed to calculate R_a. PV cells can charge the supercapacitor while providing enough energy for the load in the sleeping mode and can provide energy for the load together with the supercapacitor in active mode, which causes the supercapacitor's voltage to increase during sleeping mode and the voltage to drop during active mode. In the stable working condition, the supercapacitor's voltage changes between threshold voltages as shown in Fig. 4. Analysis for the impact factor of R_a in the two systems will help the optimization process.

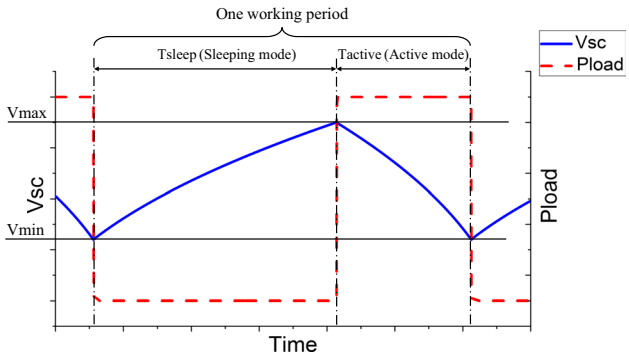

Fig. 4 Curves of V_{SC} and P_{load} over time in a stable working condition

3.1 Optimization for the non-MPPT system

T_{active} and T_{sleep} are affected by the consumption of load, operation voltage of the supercapacitor and output of PV cells. In the non-MPPT system, the consumption of load in different working modes is determined by the devices, and the operation voltage of the supercapacitor is determined by the threshold voltages shown in Fig. 4, i.e., V_{max} and V_{min}. When designing a monitoring system, the total area of PV cells is often fixed due to the restriction of the system's size. Once the number of PV cells in series increases, the area of each cell decreases. Therefore, the output voltage is in proportion to the number of cells in series, while the output current is in inverse proportion. As a result, the number of PV cells in series, indicated as N, also affects T_{active} and T_{sleep}. Among all the parameters above N,V_{max} and V_{min} are designed when optimizing the power module. Consequently, maximization of R_a is achieved by changing N and threshold voltages; the calculation process is shown in Fig. 5.

In Fig. 5, the minimum number of PV cells in series, designated N_{min}, is determined by the DCDC's lowest input voltage, dV is a voltage step in calculation, V_{oc} is the open circuit voltage of PV cells, and N_{max} is the maximum number of PV cells in series, which is determined by the supercapacitor's rated voltage. The minimum V_{min} is the start-up voltage of the DCDC, and the maximum V_{max} is the PV cells' V_{oc}. With the calculation process shown in Fig. 5, R_a can always be solved regardless of the working condition. In addition, T_{active} should be longer than the threshold time according to practical requirements, so the situations in which T_{active} is too short to transmit useful information

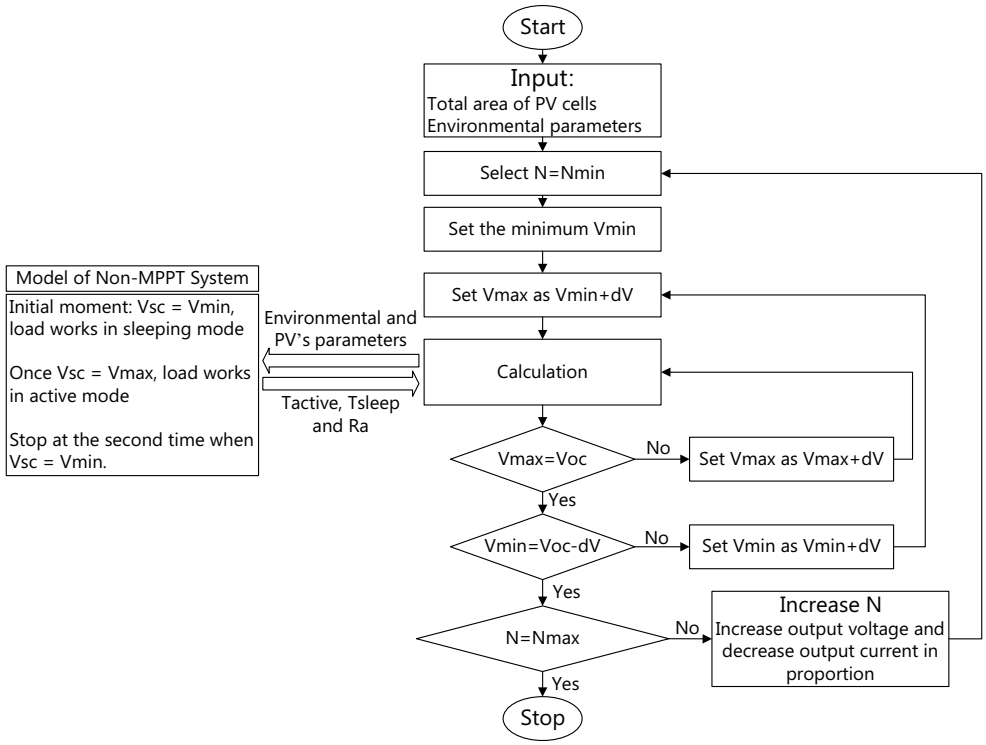

Fig. 5 Calculation process for R_a in the non-MPPT system

should be excluded. Here, $T_{a\text{-}min}$ is defined as the minimum active time, and the situations in which $T_{active} < T_{a\text{-}min}$ are excluded during the calculation process.

A set of devices are selected for simulation. PV cells are made of single-crystalline silicon. An SDM10K45-7 (Schottky Barrier Diodes, produced by Diodes Inc.) is used to protect PV cells, a CLG05P030L17 (30 mF supercapacitor, produced by Cellergy) is used to store and output energy, and a TPS62234 and a CC2530 (both are produced by TI) are selected to be the DCDC and load. Each single-crystalline silicon cell's open circuit is approximately 0.5–0.6 V, so N_{min} is 5 since TPS62234 requires at least 2 V input voltage to start up, and N_{max} is 9 since the rated voltage of CLG05P030L17 is 5.5 V. The minimum V_{min} should be higher than the start-up voltage of TPS62234, which is set as 2.1 V, and $T_{a\text{-}min}$ is set as 1 s in the optimization process.

Optimization of R_a in different environmental conditions is performed. For all conditions, the temperatures are 25 °C and air masses are 1.5, while the radiation intensity is 1000, 700, 400 and 100 W/m^2, which correspond to the ultra-high, high, low and ultra-low light intensity, respectively,

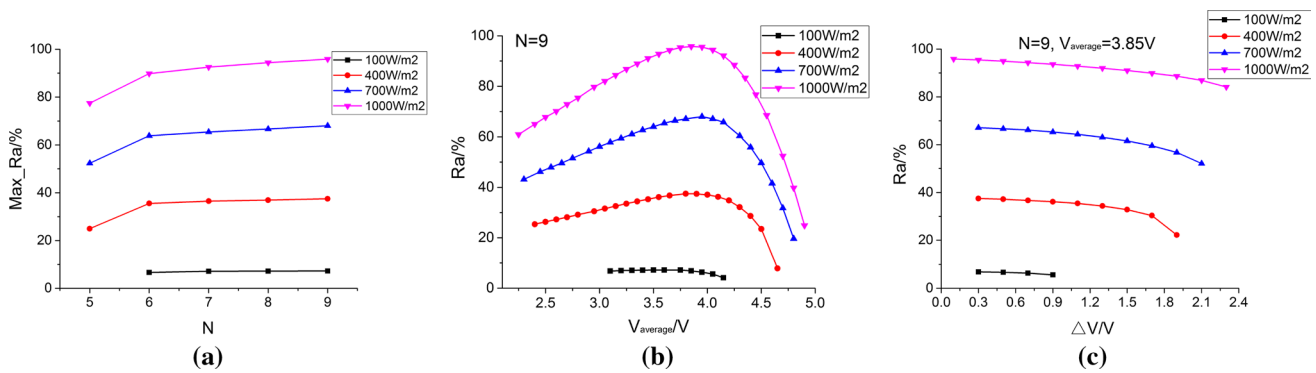

Fig. 6 R_a in different environmental conditions: **a** relationship between Max_R_a and N; **b** relationship between R_a and $V_{average}$ when N = 9; **c** relationship between R_a and ΔV when N = 9 and $V_{average} = 3.85$ V

in the natural environment (Nfah et al. 2007). The results are shown in Fig. 6, and all the raw data are provided by Online Resource.

Once N is determined, R_a is a function of V_{max} and V_{min}, and it reaches the maximum value under certain threshold voltages. The maximum value when N is fixed is indicated as Max_R_a. Figure 6a shows that there is a positive correlation between Max_R_a and N in all conditions, and Max_R_a reaches a maximum value when N = 9. The cause of this phenomenon is that the output current of PV cells is in inverse proportion to N, and the power consumption of the diode is in proportion to the current. Therefore, when N is higher, the power consumption of the diode decreases, and the power transmitted to the supercapacitor and load increases leading to a higher R_a. Figure 6b, c show the threshold voltages to reach the maximum R_a when N = 9. $V_{average}$, defined as $(V_{max} + V_{min})/2$, significantly influences R_a. Figure 6b shows that no matter how strong the radiation is, R_a reaches a relatively high value when $V_{average} = 3.85$ V. This is because there is a maximum power point (MPP) for PV cells, and it does not change very much when the radiation changes. According to Eq. 1, the average operating voltage of a supercapacitor should be close to MPP to maximize the energy collection because V_{Diode} is usually very low. Figure 6c shows that there is a negative correlation between R_a and the range of operating voltage that is indicated as ΔV, and the suitable value for different conditions is 0.3 V. The goal of minimizing ΔV is to make the operating voltage of the supercapacitor close to MPP. In conclusion, in order to maximize working efficiency, the non-MPPT system should set N = 9, $V_{average} = 3.85$ V and $\Delta V = 0.3$ V, i.e., $V_{min} = 3.7$ V and $V_{max} = 4.0$ V.

As a summary, the optimization process is achieved as follows:

Calculate R_a in different environmental conditions, as shown in Fig. 5.

Plot the maximum value of R_a as function of N, as shown in Fig. 6a. Based on the figure, determine N for the for the best system performance.

Plot R_a as function of $V_{average}$ when N is determined, as shown in Fig. 6b. Based on the figure, determine $V_{average}$ for the for the best system performance.

Plot R_a as function of ΔV when $V_{average}$ and N are determined, as shown in Fig. 6c. Based on the figure, determine ΔV for the for the best system performance.

The switch of the working modes can be achieved by using the analog-to-digital converter of the function module's microcontroller to detect V_{SC} periodically. The microcontroller turns the function module into active mode when V_{SC} rises to V_{max} and turns the function module into sleeping mode when V_{SC} falls to V_{min}.

3.2 Calculation for the MPPT system

In the MPPT system, the output power of the supercapacitor is determined by Eq. 11, which is the deformation of Eq. 10. In both the sleeping mode and active mode, P_{load}, η_{DCDC}, P_{pv}, η_{MPPT} are constant, which makes P_{SC} constant in a working mode.

$$P_{SC} = \frac{P_{load}}{\eta_{DCDC}} - P_{pv} \times \eta_{MPPT} \tag{11}$$

The input energy to the supercapacitor in the sleeping mode is equal to the output energy of the supercapacitor in the active mode, which is described in Eq. 12.

$$\begin{aligned} |P_{SC_{active}} \times T_{active}| &= \frac{1}{2}C_1(V_{max}^2 - V_{min}^2) + \frac{1}{3}K_V(V_{max}^3 - V_{min}^3) \\ &= |P_{SC_{sleep}} \times T_{sleep}| \end{aligned} \tag{12}$$

Equations 11 and 12 indicate that R_a is only affected by environmental conditions, and the function relationship is described in Eq. 13. T_{active} is determined by Eq. 14.

$$\begin{cases} R_a = {T_{active}}/{(T_{sleep} + T_{active})} = {Q_a}/{(1 + Q_a)} \\ Q_a = {T_{active}}/{T_{sleep}} = {P_{SC_{sleep}}}/{P_{SC_{active}}} \\ P_{SC_{sleep}} = P_{pv} \times \eta_{MPPT} - \frac{P_{load_{sleep}}}{\eta_{DCDC_{sleep}}} \\ P_{SC_{active}} = \frac{P_{load_{active}}}{\eta_{DCDC_{active}}} - P_{pv} \times \eta_{MPPT} \end{cases} \tag{13}$$

$$T_{active} = \frac{\frac{1}{2}C_1(V_{max}^2 - V_{min}^2) + \frac{1}{3}K_V(V_{max}^3 - V_{min}^3)}{\frac{P_{load_{active}}}{\eta_{DCDC_{active}}} - P_{pv} \times \eta_{MPPT}} \tag{14}$$

A similar set of devices are selected for calculation. The PV cells, supercapacitor, DCDC and load are the same devices as described in 3.1. MPPT is obtained by the use of FOC (Brunelli et al. 2009). The circuit includes a CPC1824 (reference PV cell, produced by IXYS Corporation), an LTC1440 (comparator, produced by Linear Technology), an LTC3401 (boost converter, produced by Linear Technology) and an SDM10K45-7, and its transfer efficiency is tested to be 85%.

According to Eq. 13, R_a is calculated to be 88.3, 61.3, 33.8 and 6.66% in the condition of ultra-high, high, low and ultra-low light intensity. The results are also listed in Table 1.

Table 1 Analysis of the two systems' simulation results

Light intensity (W/m^2)	Non-MPPT system		MPPT system	
	Total active time in 120 (s)	R_a (%)	Total active time in 120 (s)	R_a (%)
700	79.42	67.1	69.23	61.3
400	44.96	37.5	35.67	33.8

3.3 Simulation analysis

High and low light intensity are most common under natural conditions (Nfah et al. 2007), and the two systems' V_{SC}-time curves under such conditions have been simulated. The non-MPPT system's threshold voltages are set to be 3.7 and 4.0 V according to the optimization result, and the MPPT system's threshold voltages are set to the same values for comparison. The monitoring time of the systems is set to be 2 min. The simulation results in 35 s are shown in Fig. 7. Voltage behavior in total 120 s are provided by Online Resource, and Table 1 lists the analysis results.

In each condition, the loads in the two systems start with the sleeping mode where the power consumption is extremely low. The PV cells in both systems charge the supercapacitors, and V_{SC} rises at the same time. Once V_{SC} rises to V_{max}, the loads enter active mode, and the supercapacitors work together with PV cells to power the loads, which causes a decrease in V_{SC}. The loads enter sleeping mode again when V_{SC} drops to V_{min}. When the radiation becomes stronger, the sleeping time decreases and the active time increases. The reason is that when the output of PV cells is higher, the charging current of supercapacitors in sleeping mode is higher and the discharge current in the active mode is lower. The simulation results show that the non-MPPT system has more working cycles during the monitoring period, and its total active time is longer than that of the MPPT system for all conditions. More importantly, its maximum R_a is 5.8 and 3.7% higher than that of the MPPT system in the two conditions, so the conclusion that the non-MPPT system can be active longer is not only applicable to this specific monitoring time. When the monitoring time is long enough, the non-MPPT system total active time will always be longer. A longer active time means that the system has more time to sense and transmit data, so it can collect more data under the same radiation meaning higher working efficiency.

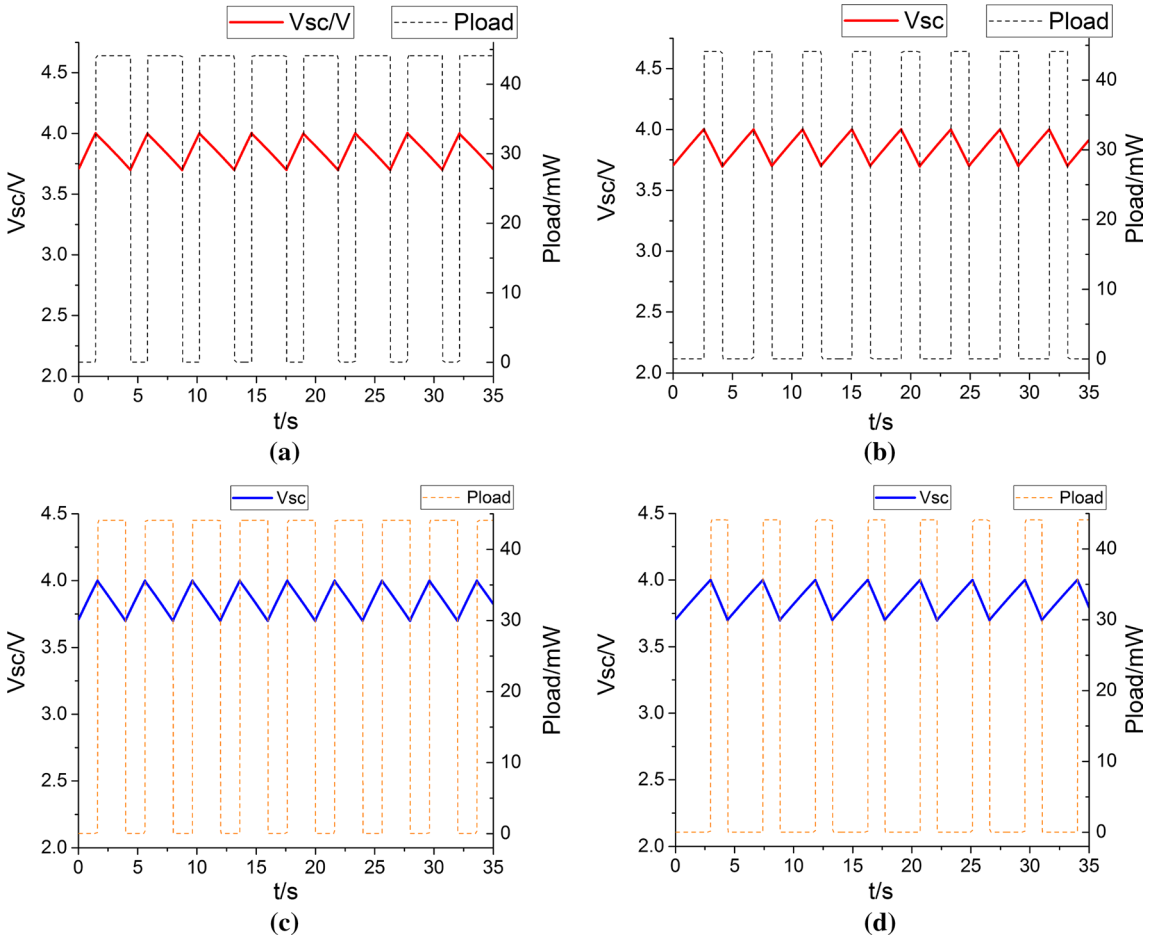

Fig. 7 Simulation results of the two similar systems in different environmental conditions: **a** results of non-MPPT system under light intensity of 700 W/m^2; **b** results of non-MPPT system under light intensity of 400 W/m^2; **c** results of MPPT system under light intensity of 700 W/m^2; **d** results of MPPT system under light intensity of 400 W/m^2

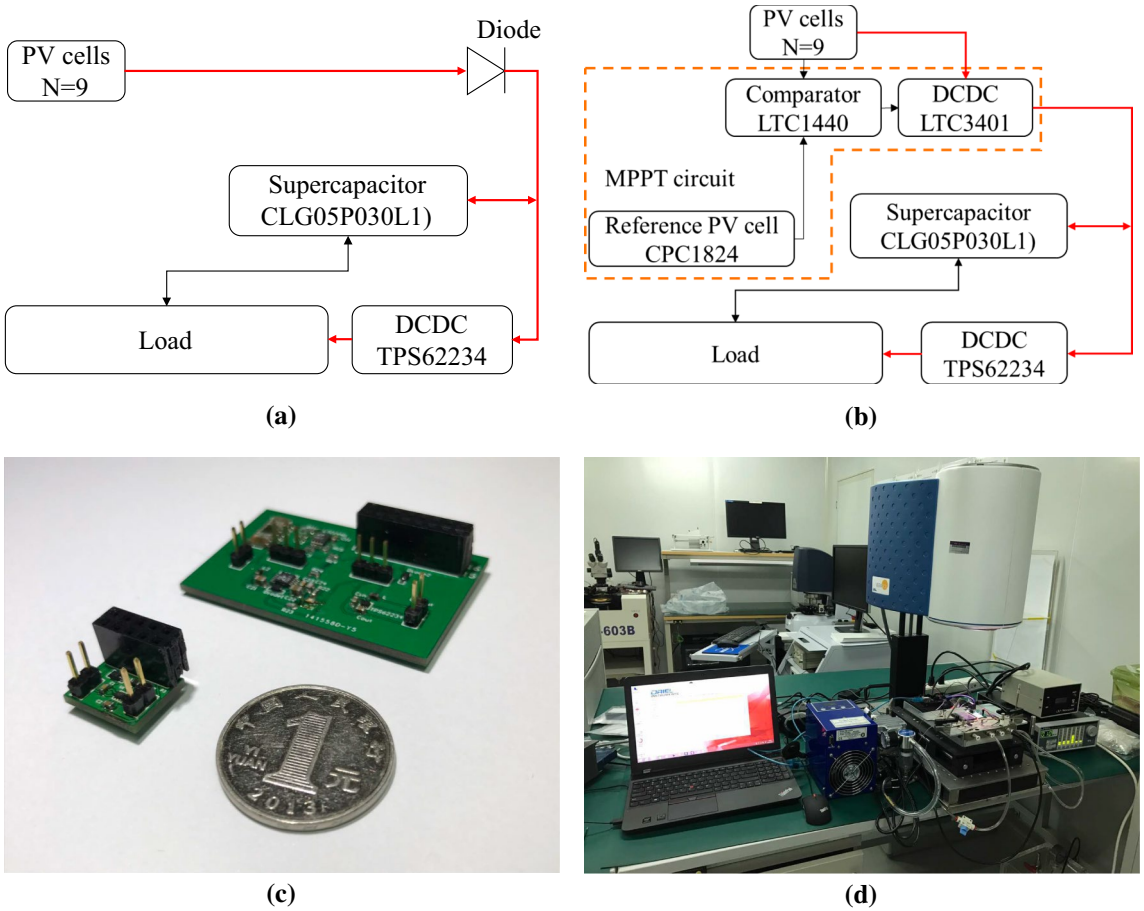

Fig. 8 **a** Block diagram of the non-MPPT system; **b** block diagram of the MPPT system; **c** circuit board for two systems; **d** experimental setup

Table 2 BOM (Bill of Material) list of the two power modules

Comment	Quantity		Component's name
	Non-MPPT system	MPPT system	
Diode	1	2	SDM10K45-7
DCDC	1	1	TPS62234
Capacitor	2	7	/
Inductor	1	2	/
Reference PV cells	0	1	CPC1824
Comparator	0	1	LTC1440
Boost converter	0	1	LTC3401
Resister	0	9	/
Total	5	24	

4 Experiment and discussion

Two systems have been developed for the experiment, and their block diagrams are shown in Fig. 8a, b. Circuits of two systems' power module are shown in Fig. 8c, where the upper board is the circuit for the MPPT system and the lower board is the circuit for the non-MPPT system. The electronic components of the two boards are listed in Table 2. The board for the MPPT system has 24 components, while the other one has only 5 components, making the system smaller and simpler. A CC2530 module and a relay module are used to simulate the load. The relay module is used to detect V_{SC}, and it connects the CC2530 and DCDC when V_{SC} rises to V_{max} to simulate the active mode power consumption of a wireless sensor node and disconnects the two parts when V_{SC} falls to V_{min} to simulate the sleeping mode power consumption. The experimental setup is shown in Fig. 8d, which includes a VeraSol (solar simulator, produced by Oriel Instruments), a myDAQ (data acquisition board, produced by NI) and a laptop.

Experiments to prove the feasibility of the model are conducted with a light intensity of 725 W/m^2. The threshold voltages of two systems are set to be 3.7 and 4.0 V, and the actual voltages has a little difference. Figure 9 shows the experimental results of the two systems in one working period, and they are compared to the simulation results.

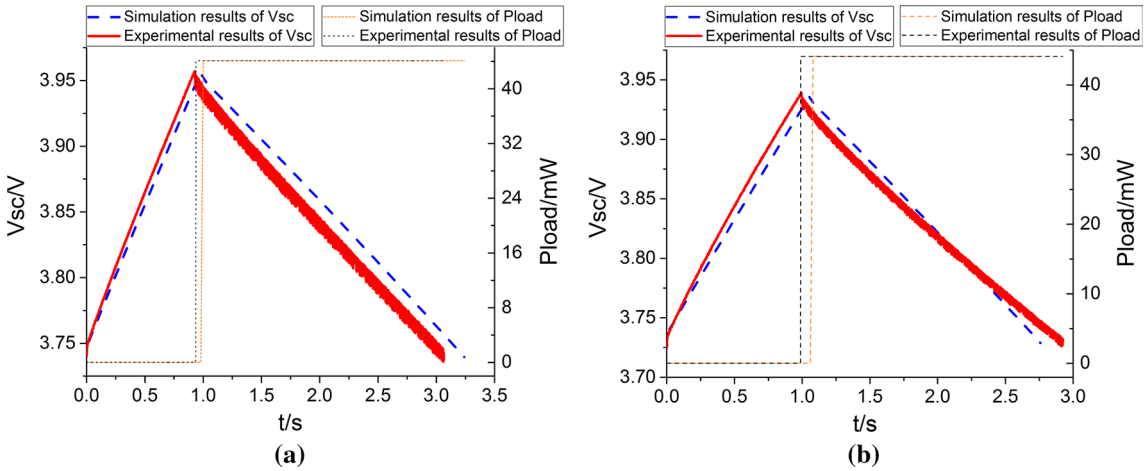

Fig. 9 Simulation and experimental results of the two similar system: **a** non-MPPT system; **b** MPPT system

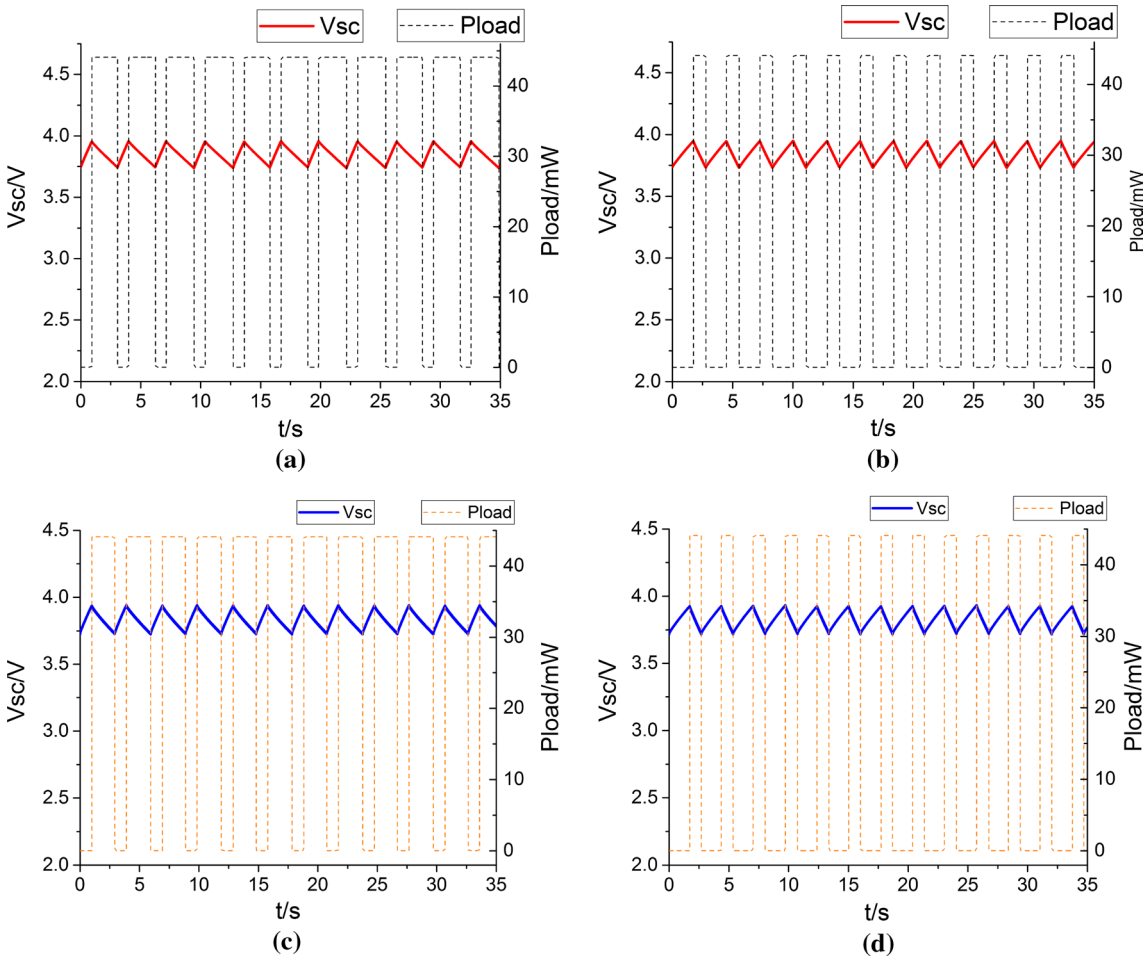

Fig. 10 Experimental results of the two similar systems in different environmental conditions: **a** results of non-MPPT system under light intensity of 725 W/m^2; **b** results of non-MPPT system under light intensity of 420 W/m^2; **c** results of MPPT system under light intensity of 725 W/m^2; **d** results of MPPT system under light intensity of 420 W/m^2

Table 3 Analysis of the two systems' experimental results

Light intensity (W/m^2)	Non-MPPT system		MPPT system	
	Total active time in 120 (s)	R_a (%)	Total active time in 120 (s)	R_a (%)
725	80.435	69.7	75.518	63.4
420	44.333	38.0	44.006	36.7

The experimental T_{sleep} in the two systems are 0.937 and 1.003 s, and the simulation results are 0.98 and 1.06 s. The experimental T_{active} values are 2.137 s and 1.93 s, and the simulation results are 2.26 and 1.74 s. The maximum relative error is less than 10%, which verifies the validity of the proposed model.

Experimental tests in the most common conditions are conducted to explore the effectiveness of the optimization result. The actual light intensity is tested to be 725 and 420 W/m^2, and the monitoring time is 2 min. The experimental results in 35 s are shown in Fig. 10. Voltage behavior in total 120 s are provided by Online Resource, and Table 3 lists the analysis results.

Experimental curves show a similar trend to the simulation curves shown in Fig. 7. Although there is a difference between the simulation and actual time duration, the experimental results of the working efficiency are very consistent with the simulation results. Table 3 indicates that the non-MPPT system can be active longer than the MPPT system during the monitoring period in the most common conditions. Its maximum R_a is 6.3 and 1.3% higher than that of the MPPT system, which indicates that the non-MPPT system can be active a little longer when the monitoring time is long enough.

According to the simulation and experimental results, the non-MPPT system has a higher R_a than the MPPT system in the most common conditions, which means its working efficiency is relatively higher. This is opposite to the common phenomenon and can be explained from the view point of energy transformation. The energy management strategy for the non-MPPT system can be regarded as a method to achieved MPPT without additional circuits, allowing PV cells to work around the maximum power point. Once the output power of PV cells is maximized, the energy transmitted to the supercapacitor and load would be close to that of the MPPT system. The conversion efficiency of the MPPT circuit is usually less than 100% that causes the harvested energy in the non-MPPT system to be slightly higher in some situations. In conclusion, no matter what devices are selected and how strong the radiation is, the working efficiency of the non-MPPT system can always be as high as that of the MPPT system with an appropriate energy strategy, and it can even be higher in some specific situations. Furthermore, our strategy is universally applicable, and it can simplify the hardware structure and reduce costs of systems with different application requirements without reducing their working efficiency.

5 Conclusion

A novel energy management strategy for wireless sensor nodes was proposed. By designing the number of PV cells in series and the working modes, the MPPT circuit for PV cells can be removed without reducing the working efficiency of a node. Models of the non-MPPT system and the MPPT system were developed for simulation. Based on real device parameters, simulations were implemented for most common conditions. The results show that the non-MPPT system's maximum R_a is slightly higher than that of the MPPT system. Experimental tests were also conducted, showing the same phenomenon that the non-MPPT system's maximum R_a is 6.3 and 1.3% higher than that of the MPPT system. All the results indicate that the working efficiency of the non-MPPT system is close to that of the MPPT system using the strategy. More importantly, the number of components in the non-MPPT system's power module is only approximately 1/5 of that of the MPPT system. This energy strategy can simplify the hardware structure of PV cell based systems and will lead to the development of wireless sensor nodes with lower cost and smaller size.

Acknowledgements This work was supported by grants from State Key Laboratory of Precision Measurement Technology and Instruments.

Compliance with ethical standards

Conflict of interest The authors declare that they have no conflict of interest.

References

Botta A, De Donato W, Persico V, Pescapé A (2016) Integration of cloud computing and internet of things: a survey. Future Gener Comput Syst 56:684–700

Brunelli D, Benini L, Moser C, Thiele L (2008) An efficient solar energy harvester for wireless sensor nodes. Proceedings of the conference on Design, automation and test in Europe. ACM, New York, pp 104–109

Brunelli D, Moser C, Thiele L, Benini L (2009) Design of a solar-harvesting circuit for batteryless embedded systems. IEEE Trans Circuits Syst I Regul Pap 56(11):2519–2528

Chou JC, Chen JT, Liao YH, Lai CH, Chen RT, Tsai YL, Chou HT (2016) Wireless sensing system for flexible arrayed potentiometric sensor based on XBee MODULE. IEEE Sens J 16(14):5588–5595

Dzimano G (2008) Modeling of photovoltaic systems. Doctoral dissertation, The Ohio State University

Enslin JHR (1990) Maximum power point tracking: a cost saving necessity in solar energy systems. Industrial Electronics Society, 1990. IECON'90., 16th Annual Conference of IEEE. IEEE, Piscataway, pp 1073–1077

Gandelli A, Mussetta M, Pirinoli P, Zich RE (2005) Optimization of integrated antennas for wireless sensor networks. In: Smart Materials, Nano-, and Micro-Smart Systems. International Society for Optics and Photonics, pp 9–15

Guan M, Wang K, Xu D, Liao WH (2017) Design and experimental investigation of a low-voltage thermoelectric energy harvesting system for wireless sensor nodes. Energy Convers Manag 138:30–37

Gubbi J, Buyya R, Marusic S, Palaniswami M (2013) Internet of Things (IoT): a vision, architectural elements, and future directions. Future Gener Comput Syst 29(7):1645–1660

Han Y, Zhang D, Zhang H, Gao Q (2008) Survey of maximum power point tracking techniques for photo-voltaic array. Int J Control Autom 9(8):49–58

Hassanalieragh M, Soyata T, Nadeau A, Sharma G (2014) Solar-supercapacitor harvesting system design for energy-aware applications. System-on-Chip Conference (SOCC), 2014 27th IEEE International. IEEE, Piscataway, pp 280–285

Jang T, Choi M, Shi Y, Lee I, Sylvester D, Blaauw D (2016) Millimeter-scale computing platform for next generation of Internet of Things. RFID (RFID), 2016 IEEE International Conference on. IEEE, Piscataway, pp 1–4

Kahn JM, Katz RH, Pister KS (1999) Next century challenges: mobile networking for "Smart Dust". Proceedings of the 5th annual ACM/IEEE international conference on Mobile computing and networking. ACM, New York, pp 271–278

Li H, Zhang G, Ma R, You Z (2014) Design and experimental evaluation on an advanced multisource energy harvesting system for wireless sensor nodes. Sci World J. doi:10.1155/2014/671280

Lu C, Raghunathan V, Roy K (2010) Maximum power point considerations in micro-scale solar energy harvesting systems. Circuits and Systems (ISCAS), proceedings of 2010 IEEE International Symposium on. Piscataway, IEEE, pp 273–276

Minami M, Morito T, Morikawa H (2005) Biscuit: a battery-less wireless sensor network system for environmental monitoring applications. In: Proceedings of the 2nd International Workshop on Networked Sensing Systems

Namisnyk A, Zhu J (2003) A survey of electrochemical super-capacitor technology. Australian Universities Power Engineering Conference. University of Canterbury, New Zealand

Nfah EM, Ngundam JM, Tchinda R (2007) Modelling of solar/diesel/battery hybrid power systems for far-north Cameroon. Renew Energy 32(5):832–844

Penella MT, Gasulla M (2007) A review of commercial energy harvesters for autonomous sensors. Instrumentation and Measurement Technology Conference Proceedings, 2007. IMTC 2007. IEEE, Piscataway, pp 1–5

Potdar V, Sharif A, Chang E (2009) Wireless sensor networks: a survey. Advanced Information Networking And Applications Workshops, 2009. WAINA'09. International Conference on. IEEE, Piscataway, pp 636–641

Raghunathan V, Kansal A, Hsu J, Friedman J, Srivastava M (2005) Design considerations for solar energy harvesting wireless embedded systems. Proceedings of the 4th international symposium on Information processing in sensor networks. IEEE, Piscataway, p 64

Razzaque MA, Dobson S (2014) Energy-efficient sensing in wireless sensor networks using compressed sensing. Sensors 14(2):2822–2859

Simjee F, Chou PH (2006) Everlast: long-life, supercapacitor-operated wireless sensor node. Low Power Electronics and Design, 2006. ISLPED'06. Proceedings of the 2006 International Symposium on. IEEE, Piscataway, pp 197–202

Zubieta L, Bonert R (2000) Characterization of double-layer capacitors for power electronics applications. IEEE Trans Ind Appl 36(1):199–205